Effect of B_2O_3 on the sintering process of vanadium–titanium magnet concentrates and hematite

Liu, Hao; Zhang, Ke; Qin, Yuelin; Saxén, Henrik; Liu, Weiqiang; Xiang, Xiaoyan

Published in:
Metals

DOI:
10.3390/met10091224

Published: 11/09/2020

Document Version
Final published version

Document License
CC BY

metals

MDPI

Article

Effect of B_2O_3 on the Sintering Process of Vanadium–Titanium Magnet Concentrates and Hematite

Hao Liu [1,2], Ke Zhang [1], Yuelin Qin [1,2,*], Henrik Saxén [3], Weiqiang Liu [3] and Xiaoyan Xiang [1,2,*]

1 School of Metallurgy and Materials Engineering, Chongqing University of Science and Technology, Chongqing 401331, China; liuhao@cqust.edu.cn (H.L.); m15902303722@163.com (K.Z.)
2 Value-Added Process and Clean Extraction of Complex Metal Mineral Resources, Chongqing Municipal Key Laboratory of Institutions of Higher Education, Chongqing 401331, China
3 Process and Systems Engineering Laboratory, Faculty of Science and Engineering, Åbo Akademi University, Biskopsgatan 8, FI-20500 Åbo, Finland; henrik.saxen@abo.fi (H.S.); weiqiang.liu@abo.fi (W.L.)
* Correspondence: qinyuelin710@163.com (Y.Q.); xxycsu@163.com (X.X.); Tel.: +86-1852-392-5702 (Y.Q.); +86-1810-830-9575 (X.X.)

Received: 30 July 2020; Accepted: 3 September 2020; Published: 11 September 2020

Abstract: This work studied the effect of B_2O_3 (analytical reagent) on the parameters of a sintering pot test, as well as the metallurgical properties and microstructure of the sinter samples, to determine the feasibility of applying solid waste containing B_2O_3 in vanadium–titanium sintering. The results show that along with B_2O_3 addition, the mechanical strength of the sinter first increases and then decreases; the maximum strength was found upon the addition of 3.0% of B_2O_3. The low-temperature reduction and pulverization rate of the vanadium–titanium sinter were also improved, while the start and end temperatures of softening showed a decreasing trend. The microstructure of the sinter was found to change from plate structure to particle and point structure, with uniformly distributed small areas. The sintering pots created by B_2O_3 addition had low total porosity but a greater pore diameter than pots created without the reagent.

Keywords: B_2O_3; vanadium–titanium sintering; metallurgical properties; microstructures

1. Introduction

Vanadium–titanium magnetite (VTM) is one of the main raw materials for extracting iron and vanadium. At present, the industrial utilization of vanadium–titanium magnetite is still based on the blast furnace-converter route. Sinter containing a high proportion of VTM concentrate exhibits a low drum strength and a high proportion of small-sized particles (<10 mm) [1]. In particular, the fracture toughness of the glass decreases with increasing titanium levels; the low-temperature reduction pulverization rate ($RDI_{-3.15}$) of VTM sinter was 40–60% higher than that of ordinary sintered ore [2,3]. Sinter with these disadvantages has caused many problems in the operation of the blast furnace.

Researchers have tried to improve the metallurgical properties of vanadium–titanium sinter by optimizing the raw materials and processes [4]. Raw material optimization may affect the central parameters and high-temperature performance [5]. The former mainly includes the chemical composition, particle size characteristics, particle morphology and water absorption of the iron ore powders [6]. The latter mainly includes assimilation, liquid phase fluidity, bonding phase strength and melting characteristics [7]. The metallurgical properties of the sinter are determined by the amount of binder phase [8–10]. Gao et al. [11] synthesized different kinds of vanadium–titanium concentrates in laboratory sintering pots to study the effects of the basicity of the raw materials, the moisture

content, the particle size of the mixture and the granulation time on the sintering of vanadium–titanium magnetite concentrates. From the perspective of mineralogy, the mass fraction of calcium ferrite in the sinter could be increased by strengthening the granulation [12]. At the same time, the mineral structures were enhanced, and the quality of the sinter was improved [13]. Higuchi et al. investigated the melting formation process via two different experimental techniques, and found that the governing factors for the melt formation of fine ores and coarse ores were different; the quantitative indices of these were estimated individually and re-combined as the sinter strength index to predict the characteristics of the whole ore mixtures [14]. Harvey et al. found that maximum temperature had a strong influence on the porosity of the fired tablets. Over-sintering caused by pore swelling may lead to a decrease in strength. The proposed mechanisms of pore swelling were bubble coalescence and gas generation from hematite decomposition to magnetite [15].

With the environmental problems brought about by wastes containing B_2O_3, such as boron mud, tailings after boron-iron beneficiation, and boric acid waste liquor, the application of these wastes in vanadium–titanium sintering has become an active field of research. Chu et al. [16] showed that indexes such as vertical sintering speed, yield, drum index, sintering cup utilization coefficient, low-temperature reduction and pulverization performance all first increase and then decrease when the mass ratio of boron ore is increased. Hao [17] found that with boric acid and calcium chloride addition, the low-temperature reduction properties and drum strength of the sinter improved, but the high-temperature reduction properties, softening temperature and softening temperature interval did not change. Zhao et al. [18] reported that when a certain amount of boron–iron concentrate was added to the vanadium–titanium sinter, the B_2O_3 could be fully utilized, the iron concentrate grains of sinter grew, the liquid phase increased, and the consolidation strength and metallurgical properties of the sinter were enhanced [19].

From the above studies, it was concluded that B_2O_3-containing materials can improve the sinter properties with vanadium–titanium magnetite as the main raw material. Therefore, the specific role of B_2O_3 has been thoroughly studied. Ren et al. [20,21] found that B_2O_3 mainly deposited in the $2CaO{\cdot}xSiO_2{\cdot}2/3(1-x)B_2O_3$ phase of high-titanium-type vanadium–titanium sinter could effectively inhibit the precipitation of $CaTiO_3$ and $2CaO{\cdot}xSiO_2{\cdot}2/3(1-x)$ B_2O_3, but promote the precipitation of iron-containing mineral phase. Zhang [22] analyzed the distribution law of the boron element in sinter-pot experiments, and found boron mainly in the glass phase of the sinter.

It is not difficult to see that boron oxide plays an essential role in the sintering process. However, earlier research mainly focused on the effect of materials containing B_2O_3 on the macro-performance of vanadium–titanium sinter. Studies on the influence of B_2O_3 on the sintering process of mixed ore powders using vanadium–titanium fine powder as the main raw material have not been reported. In particular, research on the mechanisms by which B_2O_3 influences the sintering process of the mixed ore powder of vanadium–titanium magnetite and hematite has not been reported so far.

The author earlier studied the effects of B_2O_3 on the assimilation characteristics, softening temperature, fluidity of the liquid phase, compressive strength of the bonding phase and microstructure of the mixed powder of hematite and vanadium–titanium magnetite (H-VTM) [23]. The present work was undertaken to further study the behavior of boron and its effect on sinter structure and quality. Vanadium–titanium magnetite powder and Australian hematite powder were mixed in specific ratios to form an iron ore powder (here called H-VTM) via the production recipe of a company in southwest China. H-VTM and chemical analysis reagent B_2O_3, quick lime and coke powder were used as raw materials for the sinter mix. The effects of B_2O_3 content on the sintering parameters, metallurgical properties and physical transformation of H-VTM powder were studied by using a sintering pot test device. The study was aimed at shedding light on the mechanism by which different B_2O_3 contents affected the sintering and mineralization of the H-VTM mixtures studied.

2. Materials and Methods

2.1. Raw Materials

The iron ore powder used in the experiments was obtained from the raw material site of a steel company in southwest China. For B_2O_3 an analytical reagent (≥98%) was used. The chemical composition of the raw materials is reported in Tables 1 and 2. The raw materials are mixed powder (H-VTM) composed of hematite powder and vanadium–titanium powder in a mass ratio of 2:8. As for the particle size composition of Australian hematite powder and vanadium–titanium refined powder, the grain size <1.0 mm accounted for 42.3% and 57.2%, respectively, while a 1.0–3.0 mm grain size accounted for 12.5% and 8.8%, respectively. The proportions of added B_2O_3 were 0.0%, 1.0%, 2.0%, 3.0%, 4.0% and 5.0%, expressed in wt. %. Each sintered pot test was based on 80 kg of the mixture.

Table 1. Chemical composition of sintered raw materials (wt. %).

Mixture	H-VTM	Coke Powder	Lime	B_2O_3
Ratio, wt. %	85.3	4.2	10.5	0–5

Table 2. Mixture composition.

Mineral	TFe	SiO_2	CaO	Al_2O_3	MgO	TiO_2	FeO	P	S	Loss
VTM	55.78	4.33	0.69	3.86	2.78	9.08	30.50	0.09	0.54	0.5
Hematite	59.76	4.32	0.73	3.16	0.14	0.12	0.80	0.07	0.09	6.40
Lime	-	2.46	84.85	1.53	2.26	-	-	0.02	0.06	1.0
Coke Powder	-	6.0	0.21	4.50	0.8	-	-	0.08	1.1	85

2.2. Methods

2.2.1. Sintering Pot Test Procedure

The leading test equipment used in this work is an experimental sintering set-up, which includes a mixing device, a sintering pot, Frequency modulation (FM) exhaust fan, an ignition combustion fan, a crushing device, a vibration screening and a drum test device (Figure 1). The parameters for the experimental device are given in Table 3.

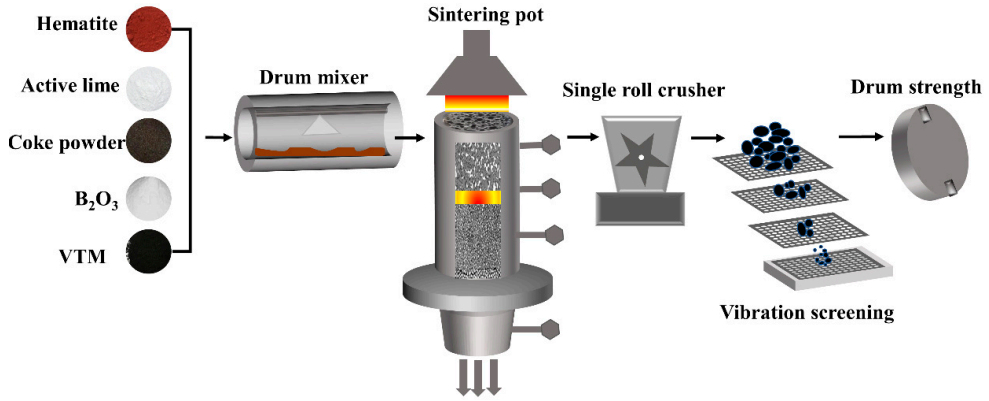

Figure 1. Flow chart of sintering pot test.

Table 3. Parameters of sintering pot.

Sintering Test Parameters	Value	Sintering Test Parameters	Value
Mixture Thickness	650 mm	Sintering Pot Diameter	300 mm
Underpressure (at the beginning)	8 kPa	Underpressure (Constant Level)	16 kPa
Ignition Temperature	1150 °C	Bottom Sinter Thickness	25 mm
Ignition Time	2 min	Granulation Time of first Mixing	2 min
Ignition Gas	Liquefied petroleum gas	Granulation Time of second Mixing	3 min
Pressure Control	FM exhaust fan	Basicity of Mixture	2

2.2.2. Metallurgical Performance Experiment

After undertaking the sintering pot test, the samples were broken, and screened samples were taken according to a certain proportion of particle size distribution to form a comprehensive sample, which were then subjected to low-temperature reduction, pulverization, reduction and soft melt dropping (Figure 2) to study the effect of B_2O_3 on the metallurgical properties of the sinter. These tests are described in the following subsections.

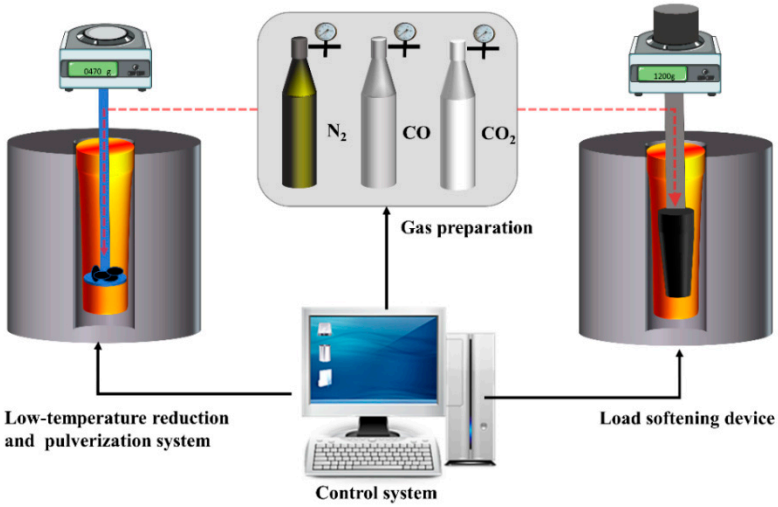

Figure 2. Schematic diagram of the metallurgical performance experimental device.

- Low-temperature reduction pulverization experiment

For sinter samples, this was done according to the national standards of China (GB/T 13242-2017 Iron ores-Low-temperature disintegration test method using cold tumbling after static reduction) [24]. The low-temperature reduction pulverization index is generally expressed as $RDI_{+3.15}$. A sinter sample with a mass of 500 ± 0.5 g and grain size of 10.0–12.5 mm was first placed in a dryer and kept there for 2 h at a temperature of 105 ± 5 °C. After this, the sample was heated at a heating rate of 10 °C/min under a protective atmosphere provided by introducing 5 L/min of N_2 into the reduction tube. When the temperature reached 500 °C, the flow of N_2 was increased to 15 L/min. The temperature was kept constant for 30 min, and during this time the gas distribution device was applied to keep the gas flow stable. After this, to start the reduction reactions, the proportions of reducing gas were 20% (CO), 20% (CO_2) and 60% (N_2). The reduction gas of 15 L/min ± 0.5 L/min was added instead of inert nitrogen. This reaction environment was maintained at a constant temperature for 1 h. At the end of the reaction, protective N_2 was introduced again, and the sample was cooled naturally at a flow rate of 5 L/min until the temperature was below 100 °C. Finally, the samples were extracted for analysis.

- Reduction index experiment

According to the national standards of China (GB/T 13241-2017 Iron ores-Determination of reducibility) [25], the reducibility measurements of the sinter samples containing B_2O_3 were undertaken in a fixed-bed reactor, under a reducing atmosphere at a high temperature. The reduction degree of the sinter was determined by the weight-loss method. First, the sinter with a grain size of 10.0–12.5 mm was sieved out to obtain a sample of 500 ± 0.5 g. This sample was placed in a blast dryer and kept there 2 h at 105 ± 5 °C. After this, the sample temperature was raised by imposing a heating rate of 10 °C/min under a protective atmosphere (N_2, 5 L/min). When the temperature in the furnace reached 900 °C, the temperature was kept constant for 30 min. Another valve was opened, letting in 30% CO and 70% (N_2) at a flow rate of 15 L/min., simultaneously with turning on the automatic monitoring system for data logging. At the end of the reaction, the reducing gas valve was closed, instead of

letting in N_2, and the sample was cooled at a flow rate of 5 L/min until the temperature was below 100 °C. Finally, the sample was extracted for examination.

- Softening and drip test under load

The softening under load was assessed to obtain information about the high-temperature behavior of the sinter. According to the national standards of China (Method for the determination of iron reduction softening dripping performance under load) [26], the test was undertaken by placing a 50 mm layer of sinter (particle size 10–12.5 mm) on 20 g of coke, and adding 15 g of coke on the top. A load of 1.0 kg/cm^2 was applied to the bed and 15 L/min of reducing gas (CO/N_2 = 30/70) was fed through the bed to heat it at a rate of 10 °C/min up to 900 °C. Then the temperature was kept constant for 60 min at 900 °C, followed by further heating (5 °C/min) until the first droplets were collected under the lower coke layer. N_2 was introduced to keep the sample below 400 °C, while reducing gas was introduced at higher temperatures. During heating, the temperature at which the height of the column experienced shrinkage by 10% was noted as the softening start temperature (T_a), the temperature at which 40% shrinkage occurs as the softening end temperature (T_e), and the softening temperature interval was determined as $\Delta T_{ea} = T_e - T_a$. Finally, T_m, the melting temperature, is defined as the temperature at which the first slag/iron droplets are observed under the lower coke layer.

3. Results and Discussion

3.1. Experimental Indicators of H-VTM Sinter of Different B_2O_3 Addition

The results of the tests undertaken in this work revealed that B_2O_3 significantly affected the key properties of the sinter. Figure 3 shows that with the increase in B_2O_3, the drum strength of the sinter increased rapidly from the initial level of 48% (0% B_2O_3) to reach a maximum value of 58.0%, when the B_2O_3 ratio was 3.0%, but decreased with the further addition of B_2O_3 to 46.7% at 5.0% B_2O_3. The vertical sintering speed increased first, then decreased, also showing a maximum at 2.0% B_2O_3. Within the range of 0.0–3.0% B_2O_3 addition, the qualified rate of sintered samples generally improved, but with B_2O_3 > 3.0%, both parameters decreased.

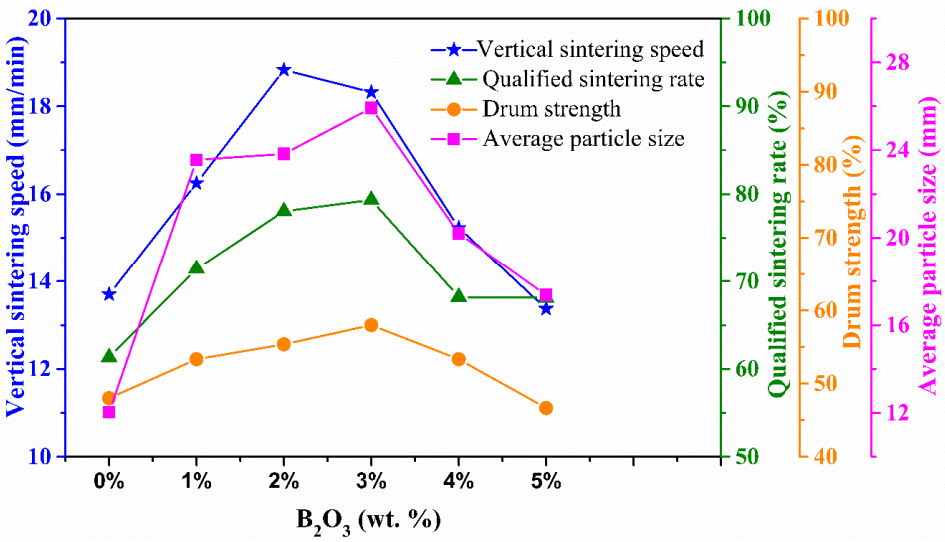

Figure 3. Key sinter properties with different additions of B_2O_3.

The overall average particle size first increased and then decreased, which is illustrated in Figure 4. Figure 5 illustrates that the particle size distribution of the sinter changed significantly with the addition of B_2O_3. The test with 1% addition of B_2O_3 reduced the share of particles <5.0 mm from 39% to 25%, and the share of >40 mm particles increased from 3% to 21%. This in practice means that the content of the bulk sinter increased strongly, and the overall particle size of the sinter also increased. A likely

reason for the observed changes is the enhanced adhesive effect caused by the increase in the liquid phase content of the sintering sample along with the increasing levels of B_2O_3. To analyze this from a theoretical perspective, the equilibrium composition was estimated by FactSage software. The results demonstrated that the liquid phase region expands when B_2O_3 is added [23]. In most of the liquid phases, B_2O_3 reacted with some of the oxides in the raw material mix to generate components with low melting points, such as $2CaO{\cdot}B_2O_3{\cdot}SiO_2$, $CaO{\cdot}B_2O_3{\cdot}2SiO_2$, $CaO{\cdot}2B_2O_3$, $CaO{\cdot}B_2O_3$, $MgO{\cdot}2B_2O_3$, $2Al_2O_3{\cdot}B_2O_3$, $CaO{\cdot}B_2O_3{\cdot}Al_2O_3$ or $2CaO{\cdot}B_2O_3{\cdot}Al_2O_3$. All these substances have melting points below 1200 °C, and hence can form liquid phases at the temperatures of the experiments [27].

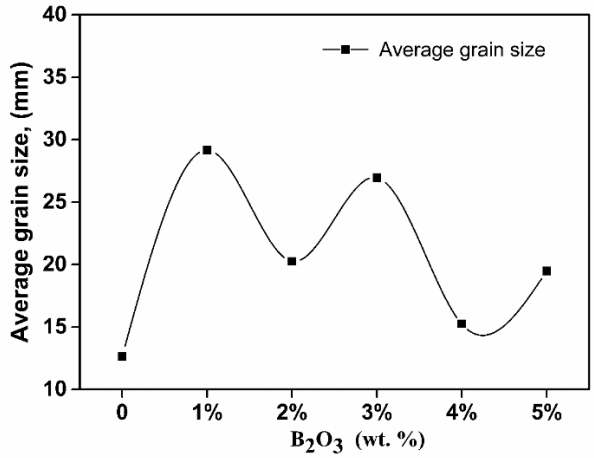

Figure 4. The average grain size of sinter with B_2O_3 addition.

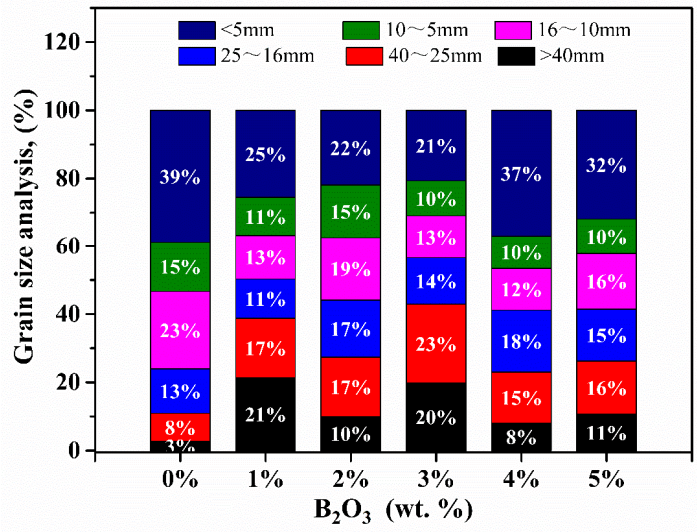

Figure 5. The size distribution of sintered ore in the sintering test for B_2O_3 addition.

When the vanadium–titanium sinter sample is cooled to 725 °C, the internal α′-$2CaO{\cdot}SiO_2$ is converted to γ-$2CaO{\cdot}SiO_2$, and its volume increases by approximately 12%. When cooled to 525 °C, β-$2CaO{\cdot}SiO_2$ changes to γ-$2CaO{\cdot}SiO_2$. During the transformation of the crystal lattice, rearrangement occurs and the density changes. Hence, the volume increases by approximately 10% during the crystal transformation. Owing to the volume expansion at cooling, the sinter is exerted by a strong force. In severe cases, this internal stress may even pulverize the sinter particles. Thus, a reduced strength may be caused by the existence of various minerals with different thermal expansion coefficients, melting points and crystallization capabilities.

The melting point of B_2O_3 is 450 °C, and its boiling point is 1860 °C. Owing to the low melting point, the addition of B_2O_3 before sintering can promote the generation of liquid crystal nuclei. Furthermore,

since the radius of the boron ion is small (0.02 nm), it can diffuse quickly into the crystal lattice of calcium orthosilicate, thereby stabilizing the crystal form of the orthosilicate, reducing the natural pulverization rate and improving the overall strength and particle size of the sample. Along with an increase in B_2O_3, the liquid phase increases. During the cooling phase, the liquid phases shrink and crystallize, and the over-melted sintered liquid phases may also froth because of the reduced surface expansion [28]. This finding applies to higher B_2O_3 contents: contents above 3% lead to large holes and thin-wall structures in the particles, as shown in Figure 6.

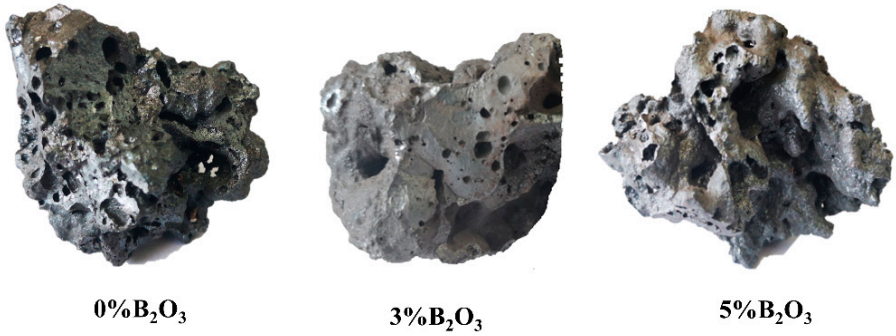

Figure 6. H-VTM sintered ore samples with different B_2O_3 addition.

3.2. *Changes in the Metallurgical Properties of the Samples for Different B_2O_3 Contents*

Before B_2O_3 was added, the low-temperature reduction pulverization index was 73.0%, but an increase of 1.0% in B_2O_3 resulted in an increase of 16.8 points to 89.8%, as shown in Figure 7. However, a further increase in the B_2O_3 content did not significantly improve the index. The addition of B_2O_3 decreased the low-temperature reduction of the smallest (−0.5 mm) fines significantly, from 11.5% to 2.6%, and thus it enhanced the ability of the sinter to resist low-temperature reduction pulverization and significantly reduced the amount of powder at low temperatures. The primary process of sintering was completed in less than 5 min, and the properties and quantity of the primary liquid phase during the sintering of vanadium and titanium were found to affect the formation of the structure of the mineral phase. The viscosity of the liquid phase is a critical factor affecting the reaction rates. The presence of B_2O_3 decreases the viscosity of the liquid phase. The liquid phase shrinks sharply during the cooling process, giving rise to pores. The effect may be indirect on pore volume and the intergranular distance of grains, as the permeability is increased and the coke burning reactions proceed more effectively. The permeability of the combustion zone was improved. This phenomenon was also beneficial to the diffusion of Ca^{2+} to the Fe_2O_3 surface in the liquid phase, allowing for the natural formation of calcium ferrite. The reduction ability and the strength of the calcium ferrite liquid phase were better than those of the silicate liquid phase and perovskite, and improved the overall resistance to pulverization of the vanadium–titanium sinter.

When more than 1.0% of B_2O_3 was added, the reducibility deteriorated clearly, since excessive liquid phases developed and the structure of the sinter became dense. The interior of the sinter melted and consolidated, and the porosity decreased, thus reducing the contact area with the reducing gas, which decreased the reduction rate.

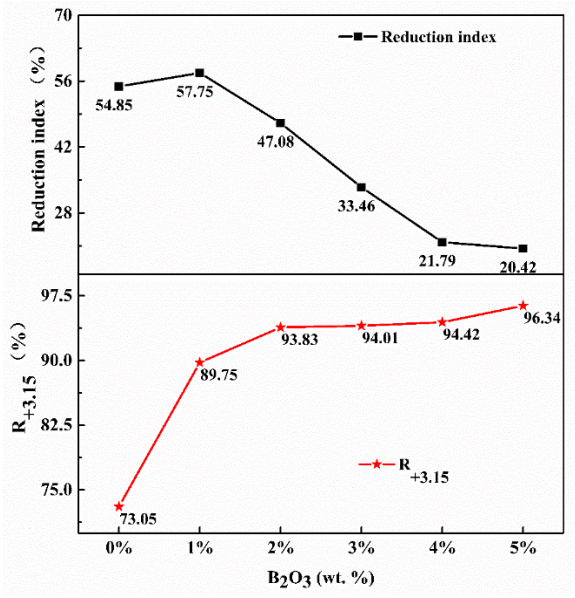

Figure 7. Metallurgical properties of sinter at B_2O_3 addition.

Figure 8 shows that after B_2O_3 addition, the melting start and end temperatures of the sinter sample decreased significantly, the melting temperature interval increased considerably, and the dripping temperature decreased. When no B_2O_3 was added, the melting temperature interval of the sinter sample was 104 °C, which increased by 110 °C with 5% B_2O_3 addition. Thus, the melting interval is strongly affected by the addition of B_2O_3 to the mixture. The reason for this is that as some free B_2O_3 exists in the sinter, its low melting point and excellent dissolution performance make it react with various metal oxides to form low melting-point compounds.

These changes are expected to give rise to an increased thickness of the cohesive zone in the blast furnace, which increases the gas flow resistance. This is not desirable since it may negatively affect the stability of the operation and the CO utilization ratio. Besides, the fact that both the softening start and end temperatures decrease causes an elevation of the vertical level of the cohesive zone, which would cause an increase in the fuel rate of the blast furnace.

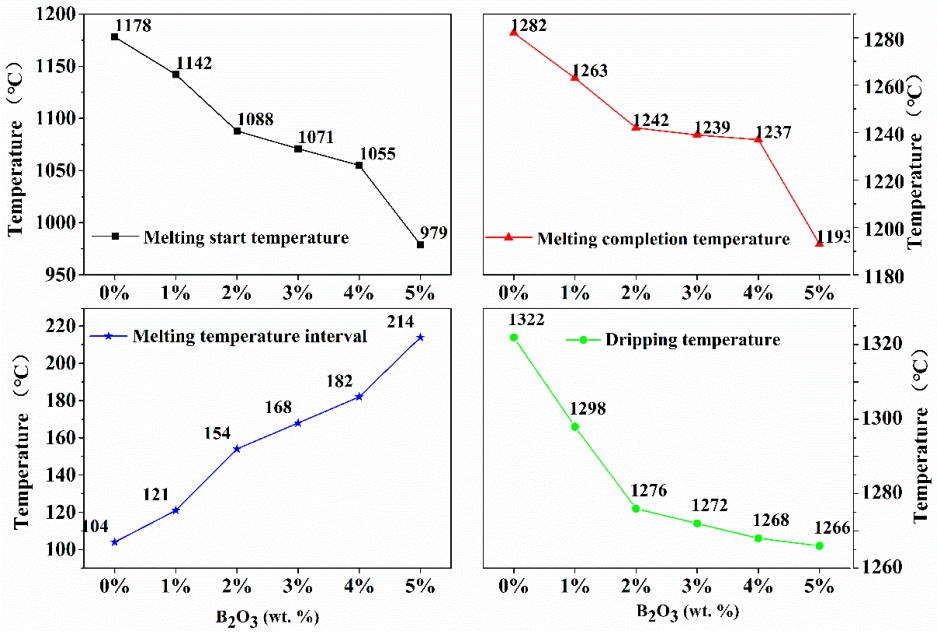

Figure 8. Melting and dripping temperatures of samples with B_2O_3 addition.

3.3. Changes in the Microstructure of the Samples for Different B_2O_3 Contents

The addition of B_2O_3 changes the sinter from a non-uniform ore phase (point, granular or dendritic) to a uniform phase (plate or block). Furthermore, B_2O_3 contributes to the formation of a liquid phase with a low melting point. As such, the amount of liquid phase generated in the crystalline phase of the sinter increases as the amount of liquid phase is increased. The enhanced liquid phase fluidity increases the scope for melting other minerals. At the same time, the presence of enough liquid phase also enhances the internal bonding ability of the sinter. The microstructure of the sinter also becomes tight, thus improving the quality of the sinter, as seen in Figure 9.

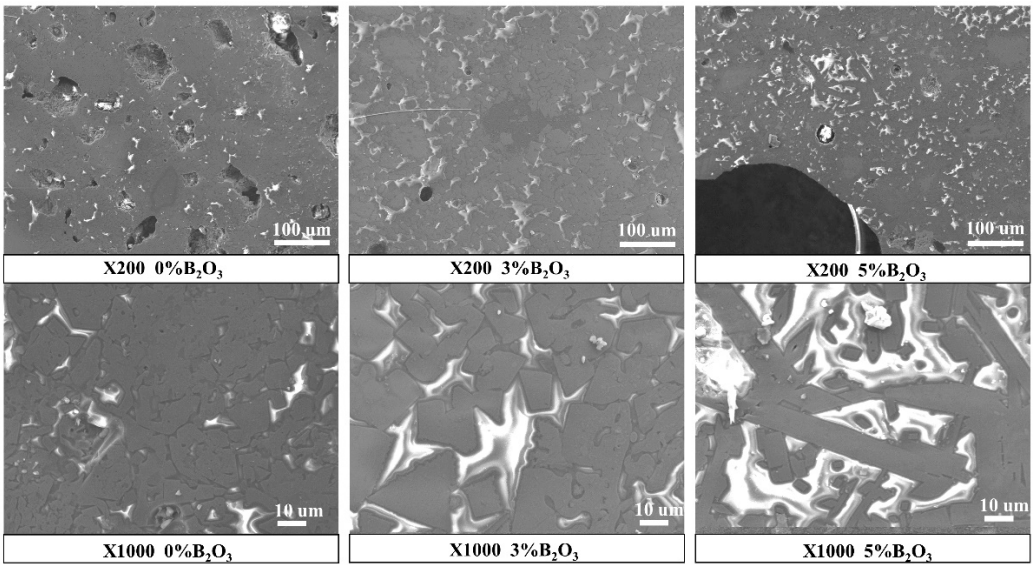

Figure 9. Scanning electron microscope (SEM) images of H-VTM at B_2O_3 addition.

When no B_2O_3 was added, the microstructure of the sinter showed poor homogeneity. Cracks were unevenly distributed and the crystal size was 0.5–1.0 mm. Another crystal phase was magnetite, appearing as small, semi-euhedral crystals with a size in the range 0.5–0.8 mm. Part of the magnetite was bound into a grain structure by dicalcium silicate, calcium, magnesium olivine and a glass phase. The calcium ferrite was plate-shaped and unevenly distributed between hematite and magnetite. A small amount of perovskite appeared and filled the region between the dendritic and magnetite particles. Dicalcium silicate was cemented between the hematite and magnetite as a dendritic phase. With the increase in the B_2O_3 content, the microstructure of the sinter changed significantly, and the mineral structure appeared uniform. The mineralogical structure of samples containing 1.0–3.0% B_2O_3 was mainly granular, partly speckle-granular, and with a skeletal structure. The hematite crystal grain size became small. The crystal grain size was 0.20–0.50 mm, and the overall porosity became small and partly uniform. However, the pore size was large and the number of cracks decreased. Hematite and magnetite were surrounded by large amounts of dicalcium silicate, and the amount of bound phase increased significantly. After adding more than 4.0% of B_2O_3, many pores appeared in the sinter, and the pores were mostly connected. When the amount was further increased, part of the hematite was found to be present as idiotypic crystals, the gaps between the grains were enlarged, and the number of bonding phases increased significantly.

As shown in Figure 10, the main elements of the mineral structure include O, Si, Ca, Ti, Fe and B, and with B_2O_3 addition, B was naturally also detected in the sinter; however, EDS surface scanning could not accurately determine its surface distribution because the atomic weight of boron is very low. The iron phase was mainly magnetite and hematite and filled with perovskite, silicate and ferrite. Mg, Al and O exhibited an even distribution in the mineral phase, and Si and Ca in the bright white area between iron the phases.

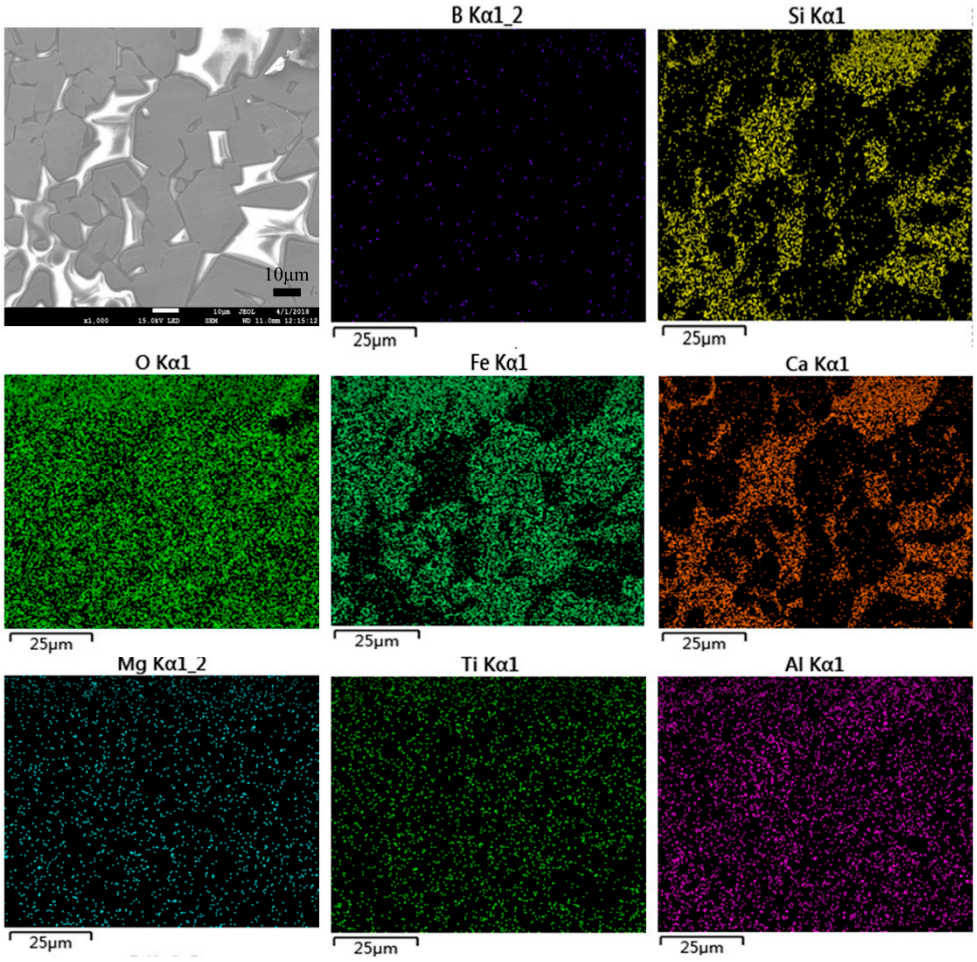

Figure 10. Surface scanning of sample with 5% B_2O_3 added.

At points A and B in Figure 11, the main elements are as shown in Table 4. The Ti content at point A was high and thus was preliminarily judged to be primary titanium magnetite. B represents the grey filled area between the iron oxide phases, and is a common area of dicalcium silicate, calcium ferrite and perovskite with enriched boron. With the gradual increase in the B_2O_3 ratio, the hematite or ilmenite gradually changed from an initial lamellar- and plate-like shape to a granular- and worm-like shape. The structure also changed from non-uniformly distributed large blocks to a uniformly distributed interlaced structure. The distribution of ferrite and titanium iron compounds was very uniform, and the structure gradually changed from a large area of plate structure to a small area of granular and dot structure. Boron was enriched in a common area of dicalcium silicate and composite calcium ferrite. Therefore, B_2O_3 significantly improved the fluidity of the binder phase and increased the total number of cohesive phases.

Table 4. SEM-EDS element content of a sample containing 5.0% of B_2O_3.

Point	Atomic Fraction (%)									
	B	**C**	**O**	**Mg**	**Al**	**Si**	**Ca**	**Ti**	**V**	**Fe**
A	1.17	5.32	26.41	0.96	3.06	0.19	0.23	3.49	0.38	58.80
B	10.19	13.01	37.84	0.97	2.72	8.83	15.67	1.96	0.22	8.59

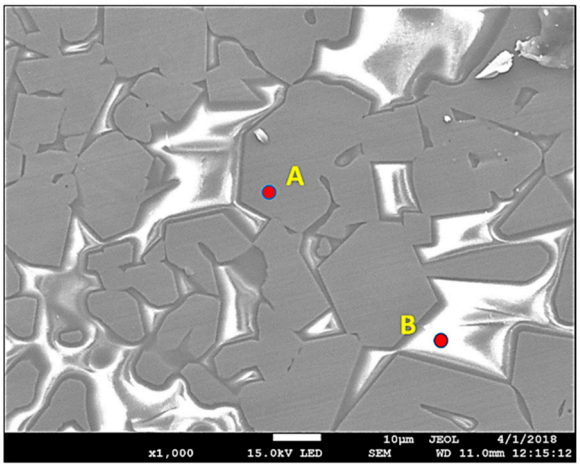

Figure 11. SEM-EDS of sinter sample adding 5% B_2O_3.

4. Conclusions

This work studied the effect of B_2O_3 on the properties of sinter produced in an 85 kg sinter test pot using 80% vanadium–titanium magnet concentrates (80 wt. %) and Australian hematite (20 wt. %). Analytical B_2O_3 was added to the sinter mix using mass ratios of 0.0–5.0% in the tests. The resulting sinter was analyzed to study the effect of boron addition. The following conclusions were drawn:

1. With B_2O_3 addition, the mechanical strength of the sinter first increased and then decreased, showing a maximum drum strength of 58% at 3.0% addition.
2. B_2O_3 addition significantly improved the low-temperature reduction pulverization of the sinter. However, when more than 1.0% was added, the improvement was limited. A low ratio of B_2O_3 was found to improve the reduction degree of the vanadium–titanium sinter, but large additions strongly reduced the reduction degree.
3. B_2O_3 addition yielded lower softening start and end temperatures of the sinter, and the softening interval grew significantly.
4. B_2O_3 addition changed the microstructure of the sinter from a large plate-like structure to a particle- and point-like structure. The total porosity was small, the diameter of the pores was large, and the number of cracks decreased.

In conclusion, the addition of boron oxide to the sinter mixture gives rise to both positive and negative effects for the resulting sinter consisting of vanadium–titanium-containing iron ores. To achieve the best performance of the sinter in the blast furnace, the addition of B_2O_3 should be limited to about 1%, so as to avoid the negative consequences of phases that melt at too low a temperature and within too wide a temperature interval.

Author Contributions: H.L., K.Z., X.X. contributed to perform the experiments, material characterization, data analysis and paper writing; H.S., W.L. and Y.Q. revised the paper and refined the language; and H.L. and Y.Q. contributed to the design of the experiment. All authors have read and agreed to the published version of the manuscript.

Funding: This work was supported by the Natural Science Foundation of Chongqing. (No. cstc2020jcyj-msxmX0583); The National Natural Science Foundation of China Grant No. 51974054); the Youth project of science and technology research program of Chongqing Education Commission of China. (No. KJQN201901); China Scholarship Council (201802075005).

Conflicts of Interest: The authors declare no conflict of interest.

References

1. Tang, W.; Yang, S.; Cheng, G.; Gao, Z.; Yang, H.; Xue, X. Effect of TiO_2 on the Sintering Behavior of Chromium-Bearing Vanadium–Titanium Magnetite. *Minerals* **2018**, *8*, 263. [CrossRef]
2. Qie, Y.N.; Lv, Q.; Zhang, X.S.; Liu, X.J.; Sun, Y.P. Effect of TiO_2 content on microstructure of sinter. *J. Iron Steel Res.* **2015**, *27*, 21–25.
3. Bristow, N.J.; Loo, C.E. Sintering Properties of lron Ore Mixes Containing Titanium. *ISIJ Int.* **1992**, *32*, 819–828. [CrossRef]
4. Zhou, M.; Yang, S.T.; Jiang, T. Influence of basicity on high-chromium vanadium–titanium magnetite sinter properties productivity and mineralogy. *JOM* **2015**, *67*, 1203–1213. [CrossRef]
5. Cores, A.; Babich, A.; Muñiz, M.; Ferreira, S.; Mochon, J. The Influence of Different Iron Ores Mixtures Composition on the Quality of Sinter. *ISIJ Int.* **2010**, *50*, 1089–1098. [CrossRef]
6. Lv, X.W.; Bai, C.G.; Qiu, G.B. Moisture capacity: Definition, measurement, and application in determining the optimal water content in granulating. *ISIJ Int.* **2010**, *50*, 695–701. [CrossRef]
7. Kasai, E.; Sakano, Y.; Kawaguchi, T.; Nakamura, T. Influence of Properties of Fluxing Materials on the Flow of MeltFormed in the Sintering Process. *ISIJ Int.* **2000**, *40*, 857–862. [CrossRef]
8. Zhou, M.; Jiang, T.; Yang, S.T.; Xue, X. Vanadium–titanium magnetite ore blend optimization for sinter strength based on iron ore basic sintering characteristics. *Int. J. Min. Proces.* **2015**, *142*, 125–133. [CrossRef]
9. Shapovalov, A.N.; Ovchinnikova, E.V.; Gorbunov, V.B.; Dema, R.R.; Kalugina, O.B. The effect of the composition of magnesia flux on the sinter structure and properties. *IOP Conf. Ser. Mater. Sci. Eng.* **2019**, *625*, 012009. [CrossRef]
10. Umadevi, T.; Nelson, K.; Mahapatra, P.C.; Prabhu, M.; Ranjan, M. Influence of magnesia on iron ore sinter properties and productivity. *Ironmak. Steelmak.* **2009**, *36*, 515–520. [CrossRef]
11. Gao, Q.J.; Wei, G.; Shen, T.S.; Jiang, X.; Zheng, H.Y.; Shen, F.M.; Liu, C.S. Influence and mechanism of Indonesia vanadium titano-magnetite on metallurgical properties of iron ore sinter. *J. Cent. South Univ.* **2017**, *24*, 2805–2812. [CrossRef]
12. Yang, S.T.; Zhou, M.; Jiang, T. Effect of sintering essential characteristics on reduction degradation index for Cr-bearing vanadium and titanium magnetite. *J. Northeast. Univ. (Nat. Sci.)* **2015**, *36*, 498–501.
13. Zhou, M.; Yang, S.T.; Jiang, T. Effect of enhanced granulation on Cr-bearing vanadium and titanium magnetite sintering. *Iron Steel* **2015**, *50*, 39–43.
14. Higuchi, K.; Okazaki, J.; Nomura, S. Influence of Melting Characteristics of Iron Ores on Strength of Sintered Ores. *ISIJ Int.* **2020**, *60*, 674–681. [CrossRef]
15. Harvey, T.; Honeyands, T.; O'dea, D.; Evans, G. Study of Sinter Strength and Pore Structure Development usingAnalogue Tests. *ISIJ Int.* **2020**, *60*, 73–83. [CrossRef]
16. Chu, M.S.; Tang, Y. Improving metallurgical properties of high chromium vanadium titanium sinter with bornite. *J. Northeast. Univ. (Nat. Sci.)* **2015**, *12*, 22–25.
17. Hao, D.S. Study on the Experiment and Mechanism of Boracic Complex Additive to the Sinter. Ph.D. Thesis, Northeastern University, Shenyang, China, 2008.
18. Zhao, Q.J.; He, C.Q.; Gao, M.H. Reasonable utilization of boronic magnetite ore. *J.Anhui Univ. Technol. (Nat. Sci.)* **1997**, *3*, 262–266.
19. Xu, J.C.; Pang, Q.H.; Me, J.W.; Zhong, Q.; Yuan, P.; Tian, C. Influence of B on the microstructure of vanadium titanium iron ore sintering. *J. Univ. Sci. Technol. Liaoning* **2016**, *39*, 401–405.
20. Ren, S.; Zhang, J.L.; Xing, X.D.; Su, B.X. Effect of B_2O_3 on phase compositions of high Ti bearing titanomagnetite sinter. *Ironmak. Steelmak.* **2014**, *41*, 500–506. [CrossRef]
21. Ren, S.; Zhang, J.L.; Liu, Q.C.; Chen, M.; Ma, X.D.; Li, K.J.; Zhao, B.J. Effect of B_2O_3 on the reduction of FeO in Ti bearing blast furnace primary slag. *Ironmak. Steelmak.* **2015**, *42*, 498–503. [CrossRef]
22. Zhang, Y.Z. Behaviour and Action Law of Boron-Magnesia Powder Agglomeration. Ph.D. Thesis, Yanshan University, Qinhuangdao, China, 2002.
23. Liu, H.; Zhang, K.; Ling, Q.F.; Qin, Y.L. Effect of B_2O_3 Content on the Sintering Basic Characteristics of Mixed Ore Powder of Vanadium–Titanium Magnetite and Hematite. *J. Chem.* **2020**, *2020*, 6279176. [CrossRef]
24. GB/T 13241-2017. *Iron Ores-Determination of Reducibility*; General Administration of Quality Supervision, Inspection and Quarantine of the People's Republic of China: Beijng, China, 2017.

25. GB/T 13242-2017. *Iron Ores-Low-Temperature Disintegration Test-Method Using Cold Tumbling after Static Reduction*; General Administration of Quality Supervision, Inspection and Quarantine of the People's Republic of China: Beijng, China, 2017.
26. GB/T 34211-2017. *Method for Determination of Iron Reduction Softening Dripping Performance under Load*; General Administration of Quality Supervision, Inspection and Quarantine of the People's Republic of China: Beijng, China, 2017.
27. Zhang, K.; Yang, Z.X. Compressive strength and reducibility of B_2O_3-MgO-SiO_2-CaO-Fe_3O_4 Agglomerate. *J. Northeast. Univ. (Nat. Sci.)* **1997**, *6*, 589–592.
28. Shigaki, I.; Sawada, M.; Maekawa, M.; Narita, K. Fundamental study of size degradation mechanism of agglomerates during reduction. *Trans. ISIJ* **2006**, *22*, 838–847. [CrossRef]